current issues in molecular biology

MDPI

Article

Sida rhombifolia L. Reduces Acute Inflammation and NF-κB/AP-1-Driven SEAP Reporter Activity in TPA- and LPS-Stimulated RAW-Blue™ Cells

Nayeli Monterrosas-Brisson [1], Enrique Jiménez-Ferrer [2], Manasés González-Cortazar [2], Valeria Beltrán-Salazar [1,2], Yury Maritza Zapata-Lopera [2], Daniel Tapia-Maruri [3], Gabriel Flores-Franco [4] and Maribel Herrera-Ruiz [2,*]

[1] Facultad de Ciencias Biológicas, Universidad Autónoma del Estado de Morelos (UAEM), Cuernavaca 62209, Morelos, Mexico; nayeli.monterrosas@uaem.mx (N.M.-B.); valeriabeltran3012@hotmail.com (V.B.-S.)
[2] Centro de Investigación Biomédica del Sur, Instituto Mexicano del Seguro Social (IMSS), Argentina 1, Xochitepec 62790, Morelos, Mexico; enriqueferrer_mx@yahoo.com (E.J.-F.); gmanases2000@gmail.com (M.G.-C.); yurymzapata@gmail.com (Y.M.Z.-L.)
[3] Centro de Desarrollo de Productos Bióticos (IPN), Calle CEPROBI 8, San Isidro, Yautepec 62731, Morelos, Mexico; dmaruri@ipn.mx
[4] Centro de Investigación en Biodiversidad y Conservación, Universidad Autónoma del Estado de Morelos (UAEM), Cuernavaca 62209, Morelos, Mexico; gabrielflores@uaem.mx
* Correspondence: cibis_herj@yahoo.com.mx; Tel.: +52-(777)-3-61-2155

Abstract

Sida rhombifolia L. is traditionally used for the treatment of conditions associated with inflammation. In this study, hexane (SrHex), ethyl acetate (SrAcOEt), and methanolic (SrMeOH) extracts were evaluated in a TPA (12-*O*-tetradecanoylphorbol-13-acetate)-induced auricular edema assay in male CF-1 mice. SrHex, the most active extract, was fractionated into H-F1–H-F5. Selected fractions were further evaluated by histological analysis and in RAW-Blue™ macrophage-derived cells stimulated with TPA or LPS (lipopolysaccharide). Cell viability and NF-κB/AP-1-driven SEAP reporter activity were determined, and fractions H-F3 and H-F5 were chemically characterized by GC-MS. SrHex showed the greatest anti-inflammatory activity among the extracts, whereas H-F3 was the most active fraction in the TPA-induced edema model. Histological and morphometric analyses showed that SrHex and fractions H-F1–H-F3 attenuated TPA-induced increases in epidermal/subcutaneous tissue thickness and collagen layer thickness. In TPA-stimulated RAW-Blue™ cells, SrHex and H-F1–H-F3 reduced NF-κB/AP-1-driven SEAP reporter activity without a substantial loss of cell viability. In LPS-stimulated cells, SrHex and H-F2–H-F5 produced concentration-dependent reductions in SEAP reporter activity while largely preserving cell viability. H-F5 showed the highest apparent potency in the reporter assay, with an IC_{50} of 20.63 µg/mL and an Emax of 98.04%. H-F1 also reduced SEAP reporter activity, although the effects at higher concentrations should be interpreted cautiously because of the concomitant reduction in the cell viability signal. A preliminary analysis by GC-MS enabled the identification of dihydroactinidiolide, 2-methylene-5α-cholestan-3β-ol, and hexanedioic acid, mono(2-ethylhexyl) ester in H-F3, whereas in the H-F5 fraction, cyclopropanetetradecanoic acid, 2-octyl-methyl ester, and 3′,8,8′-trimethoxy-3-piperidyl-2,2′-binaphthalene-1,1′,4,4′-tetrone were identified. Overall, *S. rhombifolia* showed anti-inflammatory activity in the TPA model and modulated NF-κB/AP-1-associated reporter activity in the stimulated RAW-Blue™ cells.

Check for updates

Academic Editor: Chan-Yen Kuo

Received: 28 August 2026
Revised: 8 October 2026
Accepted: 11 October 2026
Published: 22 October 2026

Copyright: © 2026 by the authors. Licensee MDPI, Basel, Switzerland. This article is an open access article distributed under the terms and conditions of the Creative Commons Attribution (CC BY) license.

Keywords: NF-κB/AP-1-driven SEAP reporter activity; phorbol esters; inflammation; culture RAW-Blue™ cells

1. Introduction

In Mexico, *Sida rhombifolia* (known locally as 'malvilla', 'barbarisco', 'escoba', or 'escobillo') is traditionally used to relieve dental pain and to treat gingivitis, gastric ulcers, and inflammatory conditions [1]. Pharmacologically, previous studies have reported anti-inflammatory effects of this species on periapical lesions in rats [2] and to inhibit the proinflammatory enzymes cyclooxygenase 1 and 2 [3]. In addition, the methanolic leaf extract of *S. rhombifolia* (300 mg/kg) showed a dose-dependent anti-inflammatory effect in a carrageenan-induced paw edema model in mice [4]. The n-hexane extract showed anti-inflammatory activity with IC_{50} values of 52.16 and 146.03 μg/mL in the NO and protein denaturation inhibition assays, respectively, in cell culture [5]. Regarding its chemical composition, several reports indicate the presence of various metabolite groups. Reported constituents include cryptolepine, vasicine, cryptolepine, vasicine, vasicinone, vasicinol, 10-methylcryptolepinone, 10-ethylcryptolepinone, quercetin 3-(2G-xylosylrutinoside), manghaslin, myricetin 7-rhamnoside, isorhamnetin 3-O-[b-D-gluco-pyranosyl-(1->2)-a L-rhamnopyranoside, peltatoside, quercimeritrin, rutin, kaempferol, tiliroside, quercetin, Isorhamnetin 3-O-[b-D-glucopyranosyl-(1->2)-a L-rhamnopyranoside, oleanolic acid, ursolic acid, β-amyrin glucoside, phytol, squalene, β-sitosterol glucoside, daucosterol, stigmasterol, β-sitosterol, γ-sitosterol, 20-hydroxy-24-hydroxymeth-ylecdysone, thamnosmonin, xanthyletin, scopoletin, scoparone, oleic acid, stearic acid, malvalic acid, linoleic acid, myristic acid, nonanoic acid, caffeic acid, 1,6-dihydroxyxanthone, rhombifoliamide, and p-hydroxyphenethyl trans-ferulate [1].

Inflammation is an adaptive response to harmful stimuli, including infection and tissue injury, and plays an essential role in host defense and tissue repair [6]. Acute inflammation is characterized by vasodilation, increased vascular permeability, and the recruitment of immune cells to the affected tissue [7]. Recognition of pathogen-associated or damage-associated molecular signals by innate immune receptors, including Toll-like receptors (TLRs) and NOD-like receptors (NLRs), activates intracellular signaling pathways involved in the inflammatory response [8]. However, when inflammatory stimuli persist or regulatory mechanisms fail, inflammation may become chronic and contribute to the development and progression of several pathological conditions [9–14].

Considering the significant ethnomedicinal use and pharmacological potential of *S. rhombifolia*, this study evaluated the anti-inflammatory effects of three extracts and selected fractions from the aerial parts of *S. rhombifolia* in a TPA-induced ear edema model, quantified inflammatory damage using histomorphometry, and measured NF-κB/AP-1-driven SEAP reporter activity in RAW-Blue™ cells stimulated with TPA or LPS. In addition, preliminary chemical profiles of the selected fractions were analyzed by GC-MS to identify several constituents.

2. Materials and Methods

2.1. Plant Material

Sida rhombifolia specimens were collected in October 2023 at the Quilamula Biological Station of the Universidad Autónoma del Estado de Morelos (UAEM), located in the Sierra de Huautla Biosphere Reserve (REBIOSH), in the Balsas River Basin, southern Morelos, Mexico (18°27′ N, 98°59′ W). A specimen was deposited in the HUMO herbarium of the Centro de Investigación en Biodiversidad y Conservación (CIByC), Universidad Autónoma

del Estado de Morelos (UAEM), where MSc. Gabriel Flores Franco performed the taxonomic identification and assigned the specimen voucher number 30276.

2.1.1. Extraction

The aerial parts of *Sida rhombifolia* L. were dried in a shaded, well-ventilated room for 30 days. Once dried, the plant material was ground using a mill (PULVEX® Mills) (Maquinaria Pulvex. Tlazintla 08710, Mexico City, Mexico), yielding 1.162 kg of dry powdered material. Sequential extraction was then performed using solvents of increasing polarity. First, 4 L of hexane were added to the ground material, and the mixture was allowed to stand for 24 h. The extract was subsequently filtered and concentrated under reduced pressure using a rotary evaporator (Heidolph™ Hei-Vap Precision HL) to obtain the hexane extract (SrHex). The residual plant material was then extracted with 4 L of ethyl acetate under the same conditions, followed by filtration and concentration under reduced pressure to obtain the ethyl acetate extract (SrAcOEt). Finally, the plant material was extracted with 5 L of methanol, and the resulting extract was filtered and concentrated to obtain the methanolic extract (SrMeOH).

2.1.2. Fractions from SrHex

The most active extract (SrHex, 10 g) was adsorbed onto silica gel (15 g) as a normal phase and fractionated on an open-column chromatography (SrC2) on a column packed with 80 g of silica gel as the stationary phase. An *n*-hexane:ethyl acetate (EtOAc) gradient was used as the mobile phase, beginning with 100% *n*-hexane and gradually increasing the proportion of EtOAc to a 50:50 *n*-hexane:EtOAc mixture, followed by 100% EtOAc and a final wash with 100% methanol (MeOH). This yielded 47 fractions of 75 mL each, which were analyzed by thin-layer chromatography (TLC) using *n*-hexane:EtOAc (70:30, *v*/*v*) as the mobile phase and visualized with ceric sulfate ($CeSO_4$). Based on similar TLC profiles, the fractions were pooled into five subfractions, designated H-F1 to H-F5.

2.1.3. Gas Chromatograph (GC) and Triple Quadrupole Mass Spectrometer (QQQ)

An Agilent Technologies 7890B gas chromatograph (Santa Clara, CA, USA) coupled to an Agilent 7000D triple-quadrupole mass spectrometer was used for GC-MS analysis. Data acquisition was performed using MassHunter Workstation software (version 12.1) in electron ionization (EI) mode. Chromatographic separation was carried out on an HP-5MS capillary column (30 m × 250 µm × 0.25 µm) coated with 5% diphenyl/95% dimethylpolysiloxane. Helium (99.9% purity) was used as the carrier gas at a constant flow rate of 1 mL/min. The injector and transfer-line temperatures were maintained at 300 °C and 310 °C, respectively. The oven temperature program was as follows: the initial temperature was set at 50 °C and held for 1 min, then increased to 300 °C at a rate of 10 °C/min and held for 1 min, followed by a final increase to 310 °C at 10 °C/min and held for 20 min. The acquired mass spectra were compared with those in the National Institute of Standards and Technology (NIST) mass spectral library for identified compounds in the H-F3 and H-F5 fractions, considering the limitations of this technology and the compounds listed in this resource [15].

2.2. Pharmacological Evaluation of Sida rhombifolia L.

2.2.1. Animals

Male CF-1 mice (25–30 g, 5–6 weeks old) were obtained from PRONAVIBE (Productora Nacional de Biológicos Veterinarios), a supplier approved by SENASICA (Servicio Nacional de Sanidad, Inocuidad y Calidad Agroalimentaria, Mexico). The animals were housed in the animal facility under a 12 h light/12 h dark cycle with artificial daylight-spectrum illumination, in cages containing sterilizable bedding made from virgin aspen and maple

hardwood (Aspen Chip bedding, NEPCO, Inc., Warrensburg, NY, USA), free of endotoxins typically associated with softwood. The environmental temperature was maintained at 25 ± 1 °C. Mice were provided with food (5001 Laboratory Rodent Diet) and clean, fresh water *ad libitum*.

Upon arrival, the animals underwent a preliminary health assessment in accordance with Mexican Official Standard NOM-062-ZOO-1999 (Technical Specifications for the Production, Care, and Use of Laboratory Animals) [16]. Animals that did not meet the predefined inclusion criteria, including appropriate body weight, normal behavioral patterns, normal fecal consistency and coloration, and healthy skin appearance, among other general health indicators, were excluded from the study and isolated from the experimental population. Animal reception, health assessment, and maintenance were supervised by a veterinary zootechnician, who ensured that only animals considered suitable for experimentation were admitted to the study. The animals were monitored for 10 days after arrival before the experimental procedures were initiated.

All animal handling and experimental procedures were conducted in accordance with NOM-062-ZOO-1999 and applicable international guidelines for the care and use of laboratory animals. The experimental protocol, including the background, justification, objectives, hypotheses, and methodology, was reviewed and approved by the Institutional Animal Care and Use Committee (CICUAL) of the Southern Biomedical Research Center (CICUAL-CIBIS) under protocol number R-CICUAL-2024-06, dated 28 June 2024.

2.2.2. TPA-Induced Auricular Edema Model

Auricular edema was induced according to the method described by Payá et al. (2010) [17]. Mice were considered the experimental units and were randomly assigned to 10 experimental groups (n = 6 per group) using the RAND function in Microsoft Excel. Each cage was labeled with the date of arrival at the animal facility, source, species, strain, sex, number of experimental units, principal investigator, collaborator, project registration number, treatment, cage number, and relevant observations. Cages were also sequentially numbered according to treatment to facilitate identification. Individual animals were identified using permanent ink markings placed at the base of the tail with Oppen animal markers.

Group sizes were based on previous studies conducted in our laboratory and were selected in accordance with the 3Rs principle of Replacement, Reduction, and Refinement [18]. A total of 60 animals were included across 10 experimental groups. Animals were enrolled according to the previously established health criteria, and no animals were excluded after the experiment had begun.

To minimize experimental bias, treatment solutions were prepared and coded by a laboratory technician who was not involved in treatment administration, thereby blinding the experimenter to treatment identity. The corresponding treatments were applied topically to the left ear of each mouse, whereas acetone was applied to the right ear as an intra-animal vehicle control. A total volume of 10 µL of each solution was applied to both the inner and outer surfaces of the ear.

Negative control (VEH: vehicle) received 2.5 µg/ear of 12-*O*-tetradecanoylphorbol-13-acetate (TPA) dissolved in acetone and applied to the left ear, whereas the right ear received acetone alone.

For the remaining groups, we administered all treatments at 1 mg/ear to the left ear and applied acetone—the vehicle used to dissolve each treatment—to the right ear.

- Positive control (INDO: indomethacin).
- Hexane extract (SrHex).
- Ethyl acetate extract (SrAcOEt).

- Methanolic extract (SrMeOH).
- Fractions derived from SrHex (H-F1, H-F2, H-F3, H-F4, H-F5).

Fifteen minutes after administration of the treatments, TPA (2.5 μg/ear) was applied to the left ear to induce acute inflammation. Four hours after TPA application, the mice were euthanized by an overdose of sodium pentobarbital (100 mg/kg, intraperitoneally), followed by cervical dislocation. Circular ear punches measuring 6 mm in diameter were collected from both the treated and untreated ears and weighed to quantify the inflammatory response. The percentage of inhibition was calculated using the following equation:

$$\Delta w = w_t - w_{nt}$$

where w_t represents the weight of the punch obtained from the treated ear and w_{nt} represents the weight of the punch obtained from the untreated ear.

The percentage inhibition of edema was calculated relative to the TPA-treated control group as follows:

$$\text{Edema inhibition}(\%) = \frac{\Delta w_{\text{control}} - \Delta w_{\text{treatment}}}{\Delta w_{\text{control}}} \times 100$$

where $\Delta w_{\text{control}}$ represents the mean ear-weight difference in the TPA-treated control group and $\Delta w_{\text{treatment}}$ represents the mean ear-weight difference in the corresponding treatment group.

No treatment-related adverse effects were observed during treatment handling, administration, or the 4 h experimental period.

To rule out a nonspecific barrier effect of the lipophilic extract SrHex, an additional group (n = 5) was included in which TPA was applied first, followed 15 min later by SrHex (1 mg/ear). Additionally, a vehicle control group (n = 5) receiving mineral oil was included to determine whether lipophilicity *per se* interfered with TPA-induced inflammation (Supplementary Material, Table S1 and Figure S1).

2.2.3. Histological Analysis

Histological analysis was performed using tissue samples obtained from the animals included in the TPA-induced ear edema experiment (n = 6). All six animals in each group were included in the histological analysis; five refers to stained sections from the middle portion of the ear per animal, not to animals selected from each group (five sections per animal; six animals per group). No animal was excluded.

Tissues were fixed in 10% phosphate-buffered formaldehyde for 1 day. They were then dehydrated in ethanol solutions of increasing concentration up to 100% and cleared with xylene. The tissue was subsequently embedded in paraffin, sectioned (5 μm), and stained using hematoxylin and eosin (H&E) and Masson's trichrome staining techniques. The stained samples, mounted on slides, were observed using an Olympus CX31 microscope. Images were captured with QCapture Pro software (Version 16.6x) at 500 μm resolution. Morphometric measurements were performed using ImageJ® software (version 1.44).

Representative microscopic fields were selected according to the same anatomical landmark and image-quality criteria across all specimens; circular ear samples (6 mm) were cut into sagittal sections, and the evaluable region was delimited from the mid-longitudinal portion of each ear to establish a sample area of 0.4 × 0.4 mm. The same procedure was applied to the five samples from each animal. Epidermal and subcutaneous tissue thickness and collagen-containing connective tissue layer thickness were each measured in triplicate for every sample.

For each parameter, the three technical measurements were averaged to obtain one value per section. The values from the five sections were then averaged to obtain one value per animal. The animal was the independent experimental unit (n = 6 per group), and animal-level values were used for the one-way ANOVA followed by Dunnett's multiple-comparison test, with the TPA-stimulated vehicle group (Veh) as the reference. Values of $p < 0.05$ were considered statistically significant. Inflammatory-cell infiltration, dermal disorganization, and vascular congestion were assessed descriptively; no numerical histological scores were assigned or statistically analyzed. Treatment assignment was not blinded during the TPA-induced inflammation model. However, prior to field selection and morphometric measurement, a researcher who did not participate in the image analysis assigned coded identifiers to the slides. The observer was unaware of the treatment assignment, and the code was not revealed until the morphometric analysis was completed.

2.2.4. RAW-Blue™ Macrophage-Derived Cells Experiments

RAW-Blue™ cells were cultured according to the manufacturer's recommendations (InvivoGen, San Diego, CA, USA). These cells are derived from murine RAW 264.7 macrophages and contain a secreted embryonic alkaline phosphatase (SEAP) reporter gene under the control of NF-κB/AP-1-inducible elements. Accordingly, RAW-Blue™ cells were used to monitor NF-κB/AP-1-associated signaling in response to inflammatory stimuli, including LPS and TPA.

Before the cellular experiments, SrHex and its derived fractions were lyophilized to remove the organic solvents used during extraction and chromatographic fractionation. The dried samples were then reconstituted in 0.002% Tween, sonicated for 1 h to improve dispersion, and passed through a 40 μm filter before being applied to the cell cultures.

Cells were counted using a Neubauer hemocytometer and seeded at approximately 5×10^4 cells per well. After seeding, cells were allowed to adhere and stabilize for 12 h under standard culture conditions. The cells were then exposed to the corresponding concentrations of SrHex or its fractions for 1 h before LPS or TPA stimulation. Following stimulation, cultures were incubated for an additional 24 h at 37 °C in a humidified atmosphere containing 5% CO_2.

For the TPA-stimulated experiments, SrHex was evaluated at 200 and 500 μg/mL, and H-F1, H-F2, and H-F3 were evaluated at 25, 50, and 100 μg/mL. For the LPS-stimulated experiments, SrHex was evaluated at 125, 250, 500, and 800 μg/mL, and fractions H-F1–H-F5 were evaluated at 25, 50, 100, 200, 400, and 800 μg/mL.

After the 24 h incubation period, 50 μL of culture supernatant was collected from each well and mixed with 150 μL of QUANTI-Blue™ reagent. The reaction was incubated for 30 min, and NF-κB/AP-1-driven SEAP reporter activity was determined spectrophotometrically by measuring absorbance at 630 nm.

Vehicle-treated unstimulated cells were used to establish basal reporter activity. Vehicle-treated cells stimulated with LPS or TPA served as the inflammatory stimulus control. Cultures treated with SrHex or the corresponding fractions in the absence of inflammatory stimulation were included to evaluate treatment-related effects independent of LPS or TPA. Indomethacin (INDO; 200 μg/mL) was used as the reference anti-inflammatory treatment.

There were three independent replicates (N = 3). Experiments were repeated on different days and with different passages to ensure biological variation.

The culture medium served as the control, and the supernatant from LPS-stimulated cells was set to 100% activity. The percentage of inhibition of SEAP reporter activity as an indirect measure of NF-κB-related signaling (%) was calculated as follows:

$$Inh\ (\%) = \left(\frac{A - B}{A}\right) \times 100$$

where *Inh* is the inhibition of SEAP reporter activity (%), *A* is the O.D. (at 630 nm) of the group with only LPS, and *B* is the O.D. (at 630 nm) of the treatment.

SEAP reporter activity was not normalized to cell viability, viable cell number, or total protein content. Cell viability was evaluated separately as an independent assay to assess potential treatment-related cytotoxicity. Therefore, SEAP reporter activity represents the directly measured extracellular reporter signal under each experimental condition.

For graphical representation, SEAP reporter activity was expressed relative to the LPS-stimulated control, which was defined as 100%. This normalization was performed only with respect to the LPS-stimulated reference group and was not adjusted for cell viability, viable cell number, or total protein content.

$$\text{Normalized activity} = \frac{OD_{treatment} - OD_{Veh}}{OD_{LPS} - OD_{Veh}} \times 100$$

The TPA assay was used primarily for activity screening, using lower concentrations for the SrHex-derived fractions. In contrast, the LPS experiments used a broader concentration range to characterize concentration-dependent responses and calculate the inhibitory concentration (IC_{50}) and maximum observed inhibition (Emax). The percentage of inhibition for each treatment was plotted to generate the concentration–response curve. The data were plotted on a semi-logarithmic scale (effect vs. log concentration), and the resulting points were fitted to a linear regression model (y = mx + b). The 50% inhibition value was then interpolated from the regression equation to estimate the half-maximal inhibitory concentration (IC_{50}).

2.2.5. Cell Viability Assay

RAW-Blue™ cells were seeded and treated with different concentrations of *S. rhombifolia* extract for 24 h. After treatment, cells were incubated with MTT for 2 h. The formazan crystals were dissolved in DMSO, and the absorbance was determined at 490 nm using a plate reader (BioTek Instruments, Winooski, VT, USA).

2.3. Statistical Analysis

Data from the TPA-induced ear edema, RAW-Blue™ reporter assays are expressed as mean ± standard deviation (SD) and were analyzed by one-way analysis of variance (ANOVA) followed by Dunnett's post hoc test for a comparison with the vehicle control group. Statistical significance was set at $p \leq 0.05$.

Quantitative morphometric data were analyzed at the animal level (n = 6 per group) using one-way ANOVA followed by Dunnett's multiple-comparison test, with the TPA-stimulated vehicle group as the reference $p \leq 0.05$.

3. Results

3.1. Yield of the Extract and Fractions

Maceration of 1162 g of dried aerial parts of *S. rhombifolia* yielded 12 g of hexane extract (SrHex; 1.03%), 83.2 g of ethyl acetate extract (SrAcOEt; 7.16%), and 176.62 g of methanolic extract (SrMeOH; 15.2%). Thin-layer chromatography (TLC) of SrHex and its derived fractions H-F1–H-F5 revealed chromatographic bands consistent with the presence

of hydrocarbons, terpenes, cholestane-type compounds, naphthoquinones, and carboxylic acid esters. Comparison with a β-sitosterol reference standard showed a band with similar chromatographic behavior in fraction H-F2 (Figure 1).

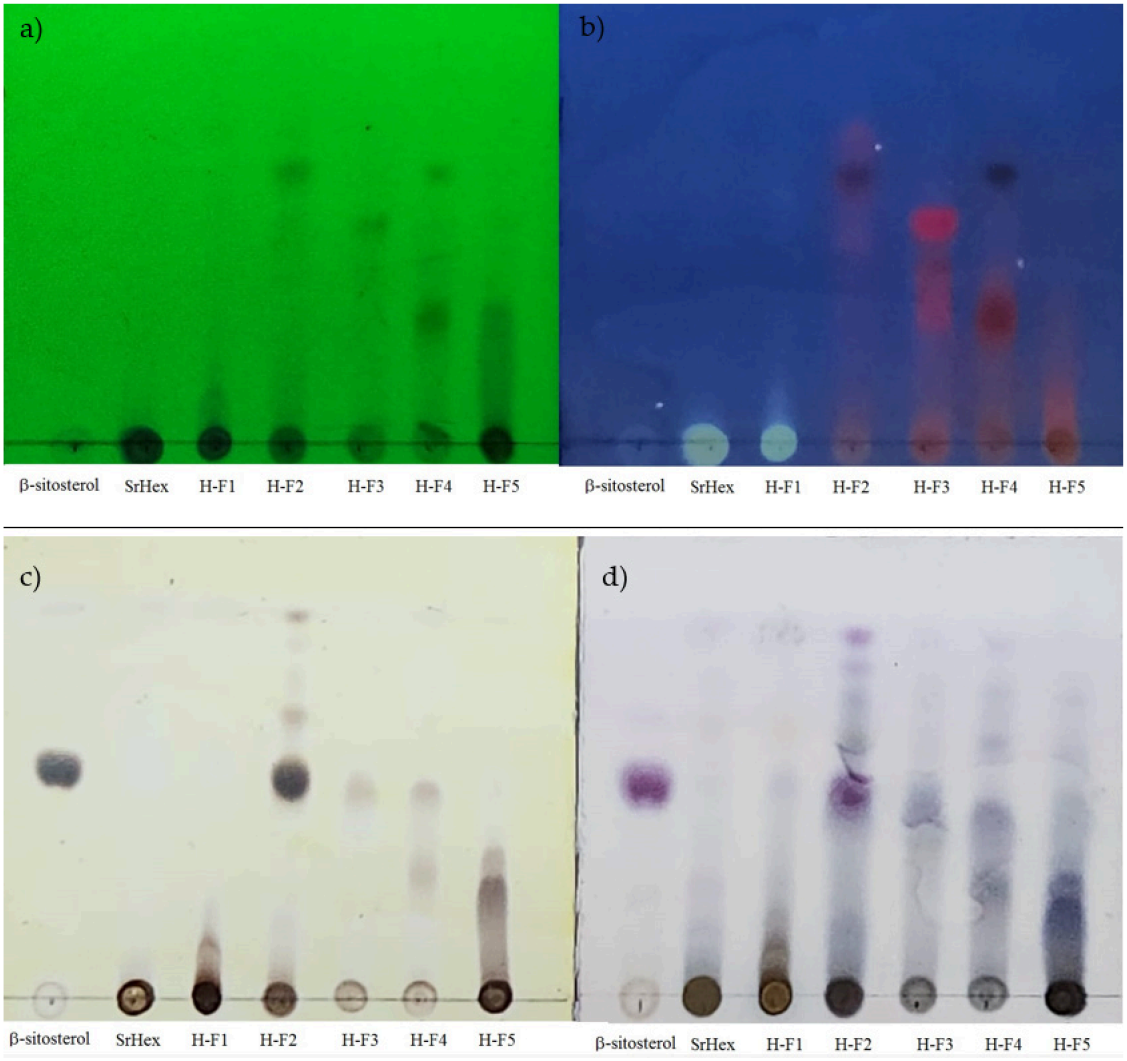
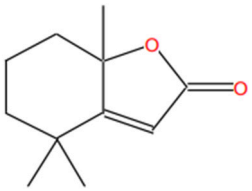
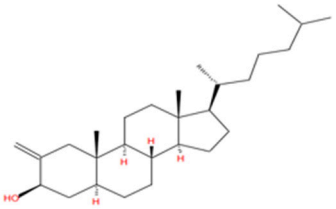
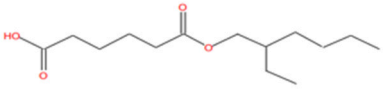
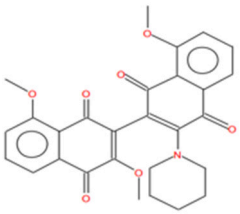


Figure 1. Thin-layer chromatography. The 70:30 hexane/ethyl acetate system was compared with the β-sitosterol, hexane extract, and fractions: (**a**) UV at 254 nm, (**b**) UV at 366 nm, (**c**) visualized with ammoniacal ceric sulfate, and (**d**) visualized with 4-hydroxybenzaldehyde.

3.2. Chemical Identification of the H-F3 and H-F5 Fractions

Table 1 presents the GC-MS results providing an assessment of the chemical composition of fractions H-F3 and H-F5; these results are preliminary and require further investigation to separate these fractions more precisely and ultimately isolate the pure compounds. In H-F3, dihydroactinidiolide, a norisoprenoid, appeared to be the predominant constituent among the compounds detected, together with the cholestane derivative 2-methylene-5α-cholestan-3β-ol and the dicarboxylic acid ester hexanedioic acid, mono(2-ethylhexyl) ester. In H-F5, cyclopropanetetradecanoic acid, 2-octyl-methyl ester, a fatty acid ester, and 3′,8,8′-trimethoxy-3-piperidyl-2,2′-binaphthalene-1,1′,4,4′-tetrone, a naphthoquinone-type compound, were identified based on their GC-MS profiles and spectral library matches, providing an initial characterization of the chemical constituents of this fraction.

Table 1. Preliminary composition by GC-MS analysis of the H-F3 and H-F5 fractions of *Sida rhombifolia* L.

Number	Compound Name	Retention Time (min)	Relative Area Abundance (%)	Molecular Weight (g/mol)	Chemical Structure
			Fraction H-F3		
1	2(4H)-Benzofuranone, 5,6,7,7a-tetrahydro-4,4,7a-trimethyl-, (R)- (dihydroactinidolide)	15.88	65.19	180.24	
2	Cholestan-3-ol, 2-methylene-, (3β,5α)-	19.28	12.11	400.7	
3	hexanedioic acid, mono(2-ethylhexyl)ester	23.92	22.68	258.35	
			Fraction H-F5		
1	Cyclopropanetetradecanoic acid, 2-octyl-, methyl ester	23.93	59.17	394.67	
2	3′,8,8′-trimethoxy-3-piperidyl-2,2′-binaphthalene-1,1′, 4,4′-tetrone	25.89	40.82	487.5	

3.3. Anti-Inflammatory Effect of S. rhombifolia L. Extracts and Fractions on TPA-Induced Edema Model

Figure 2 shows that TPA produced a mean ear-weight difference of 12.3 mg in the VEH group. Indomethacin (INDO; 1 mg/ear) inhibited edema by 87.3%. Both data points were statistically significant (* $p \leq 0.05$). SrHex and SrMeOH extracts reduced TPA-induced edema significantly compared to VEH (* $p \leq 0.05$; Figure 1), showing inhibition percentages of 69.6% and 56.8%, respectively. SrAcOEt had no significant effect on inflammation compared to VEH ($p > 0.05$). SrHex fractionation yielded five fractions with anti-inflammatory activity, as shown in Figure 1. The five treatments reduced edema significantly (* $p \leq 0.05$), with H-F3 displaying the highest activity. Percentages of reductions by each fraction were H-F1 58.4%, H-F2 62.8%, H-F3 77.06%, H-F4 53.3%, and H-F5 42.5%.

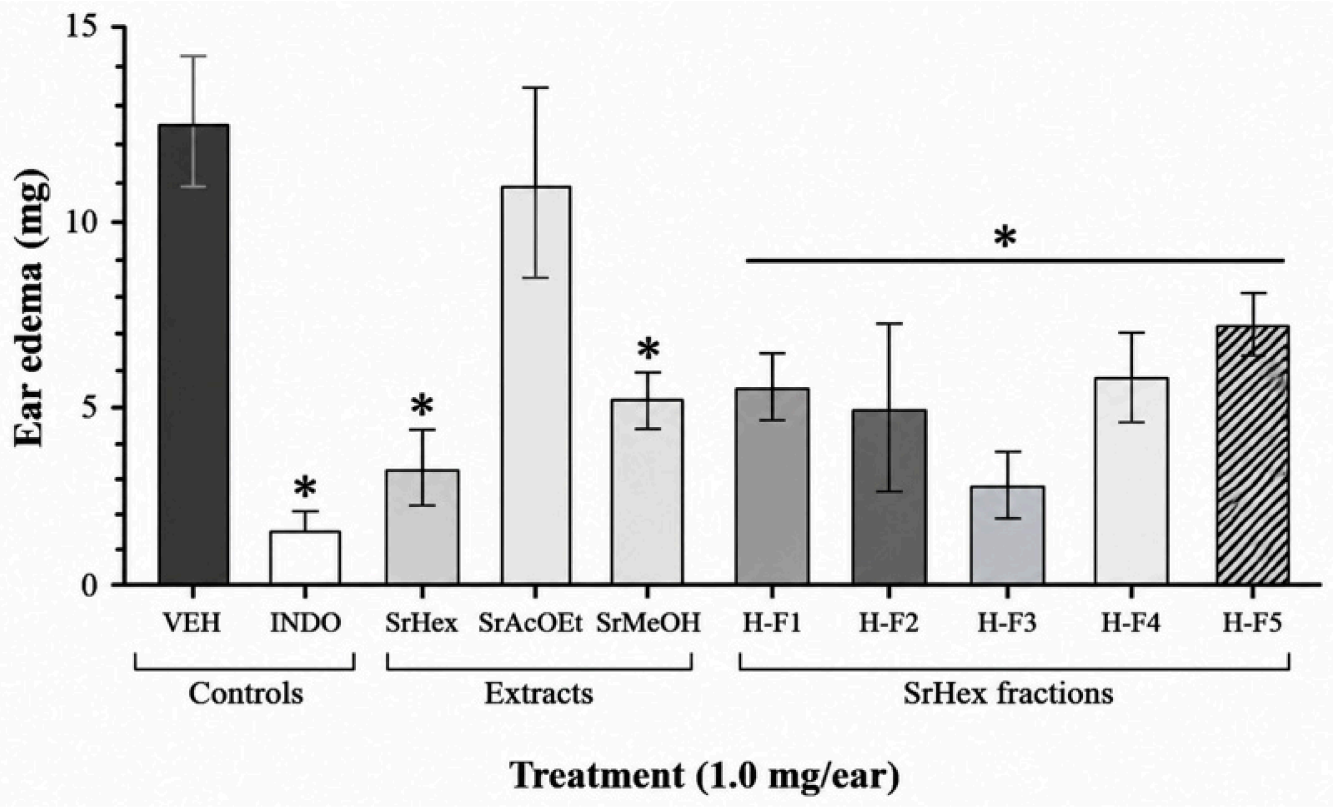


Figure 2. Anti-inflammatory effect of the *Sida rhombifolia* L. extracts and SrHex-derived fractions on TPA-induced auricular edema in mice. Effects of topical administration of the hexane (SrHex), ethyl acetate (SrAcOEt), and methanolic (SrMeOH) extracts of *S. rhombifolia* L., as well as the SrHex-derived fractions H-F1, H-F2, H-F3, H-F4, and H-F5, on ear edema induced by 12-*O*-tetradecanoylphorbol-13-acetate (TPA). Data are expressed as the mean ± SD (n = 6). Statistical analysis was performed using one-way ANOVA followed by Dunnett's multiple-comparison test. * $p \leq 0.05$ versus the TPA-stimulated vehicle (VEH) group.

3.4. Histological Analysis of the Effect of S. rhombifolia L. on TPA-Induced Auricular Edema

SrHex and fractions H-F1, H-F2, and H-F3 showed the most favorable responses among the plant-derived treatments in the TPA-induced inflammation model and were therefore selected for histomorphometric analysis. As shown in Figure 3, these treatments and the reference drug indomethacin (INDO) attenuated the histopathological alterations to varying degrees. Compared with the vehicle control group, treated tissues exhibited less epidermal and subcutaneous thickening and better-preserved dermal architecture. Among the fractions evaluated, H-F3 showed particularly evident improvements in tissue organization, including reduced epidermal/subcutaneous tissue thickness and a thinner collagen-containing connective tissue layer.

Overall, the histological and morphometric findings indicate that SrHex and its active fractions attenuated TPA-induced structural alterations in ear tissue. Among the fractions evaluated, H-F3 showed the most pronounced reductions in tissue thickening and collagen-containing connective tissue layer thickness, with values approaching those observed following indomethacin treatment.

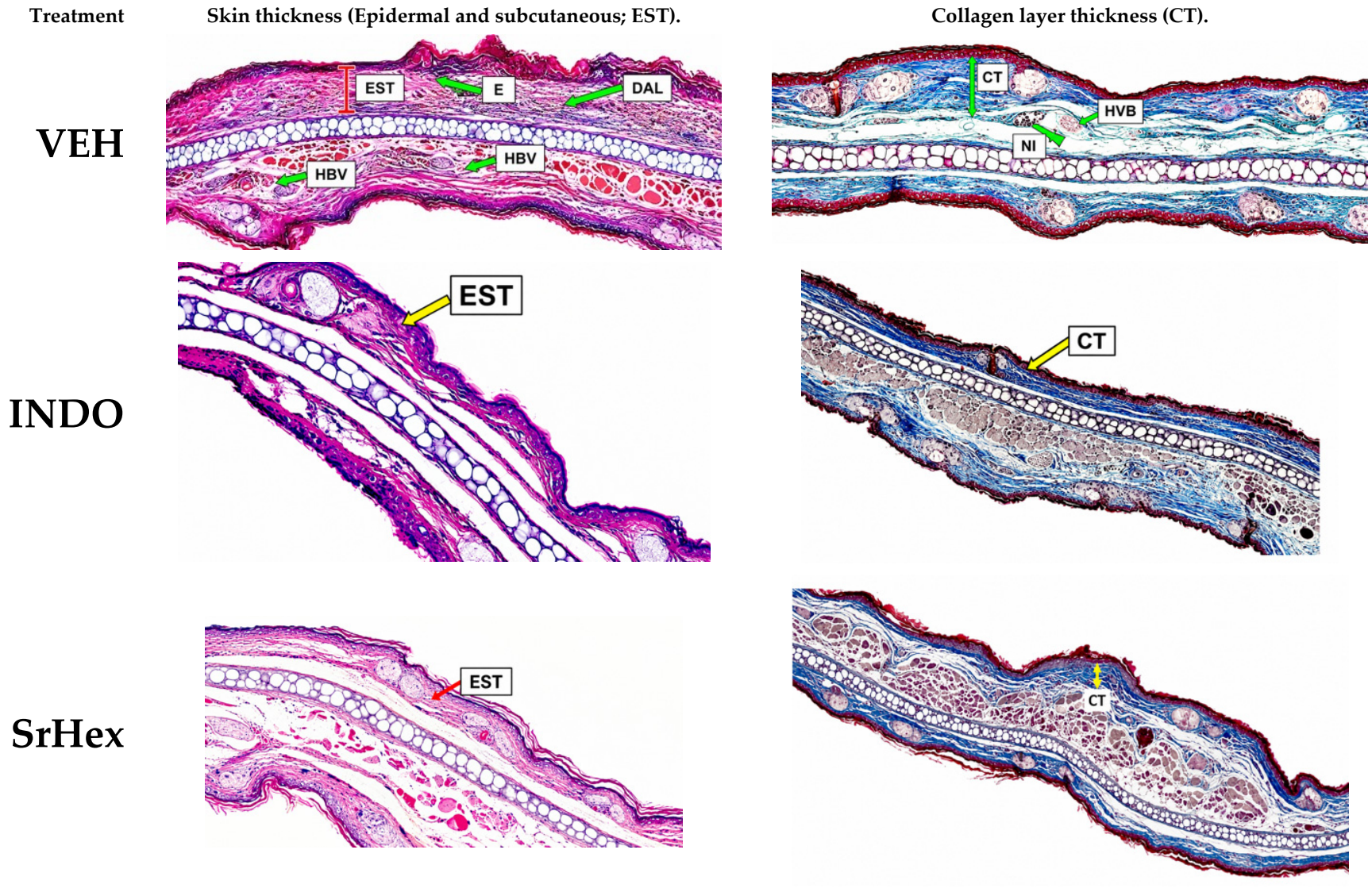


Figure 3. *Cont.*

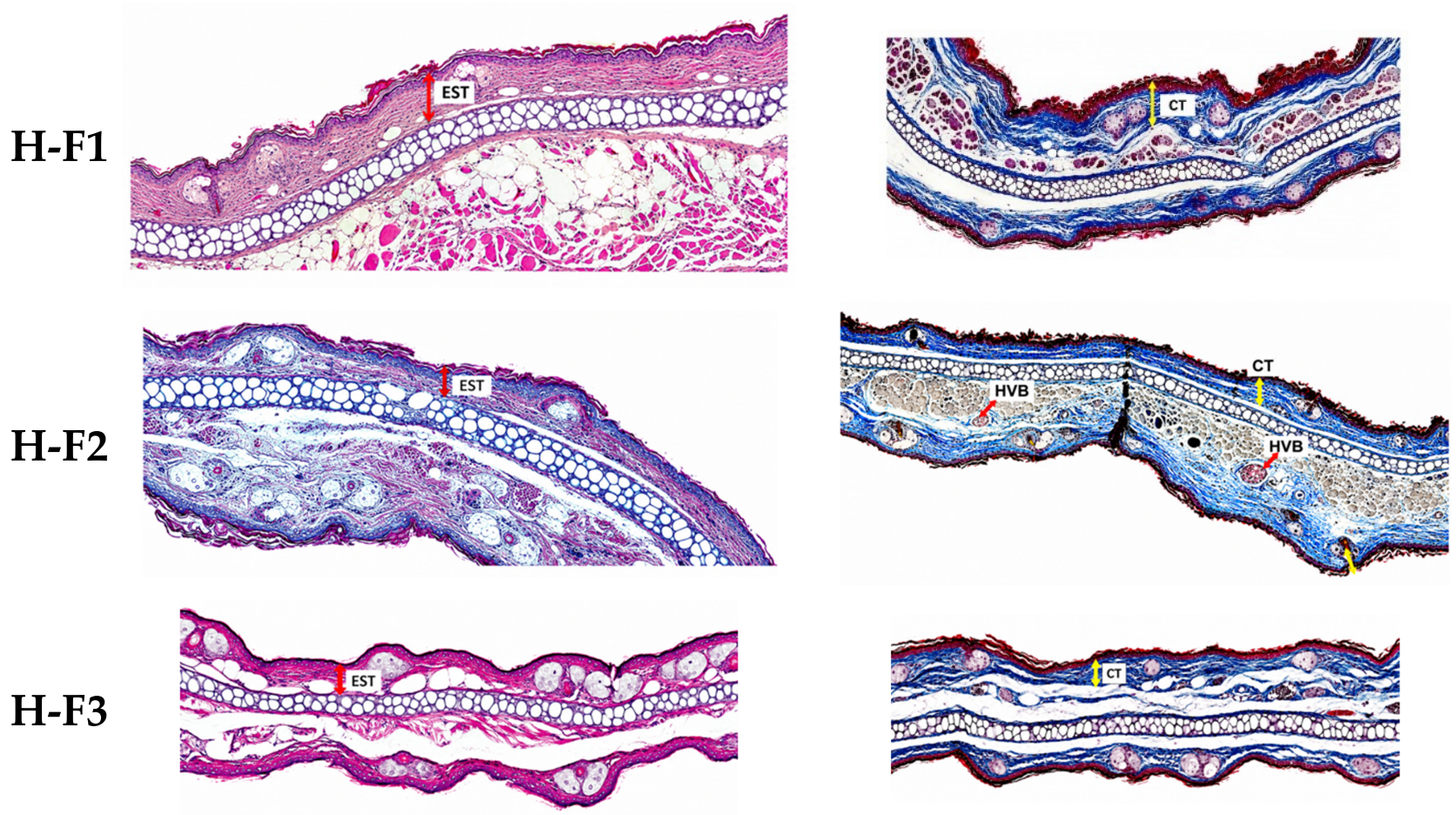


Figure 3. Histological effects of the hexane extract of *Sida rhombifolia* L. (SrHex) and selected fractions on TPA-induced auricular inflammation. Representative histological sections from different groups (n = 5): vehicle (VEH), indomethacin (INDO), SrHex, H-F1, H-F2, and H-F3 treatment groups. Histopathological parameters included epidermal and subcutaneous tissue thickness (EST), neutrophil infiltration (NI), disorganization of the reticular dermis (DAL), vascular congestion characterized by hyperemic blood vessels (HBVs), and collagen layer thickness (CT). TPA induced marked tissue thickening, inflammatory cell infiltration, dermal disorganization, vascular congestion, and increased collagen-containing connective tissue thickness. Treatment with INDO, SrHex, and the selected fractions attenuated these histopathological alterations, with H-F3 showing a marked improvement in tissue architecture.

Histological parameters associated with TPA-induced inflammation observed in the vehicle-treated (VEH) ears, specifically epidermis and subdermal tissue thickening and collagen-containing connective tissue layer thickness, significantly decreased from 498.7 ± 12 µm to 225 ± 6.3 µm with indomethacin treatment (INDO) (* $p \leq 0.05$). The SrHex extract (SrHex), as well as its purified fractions H-F1, H-F2, and H-F3, reduced hyperplasia to 352 ± 20 µm, 430 ± 27 µm, 390 ± 9 µm, and 353 ± 8 µm, respectively, compared to the VEH group (Figure 4a; * $p \leq 0.05$). Collagen-containing connective tissue layer thickness, estimated by measuring collagen deposition thickness, was thinner in the SrHex (43.4 ± 7 µm), H-F1 (74.3 ± 3.2 µm), H-F2 (63.8 ± 2.4 µm), and H-F3 (44.8 ± 2.5 µm) ears than in the VEH group (85.6 ± 1.97 µm), while the INDO value was 36.9 ± 3.7 µm; all groups were different in comparison to VEH (Figure 4b; * $p \leq 0.05$).

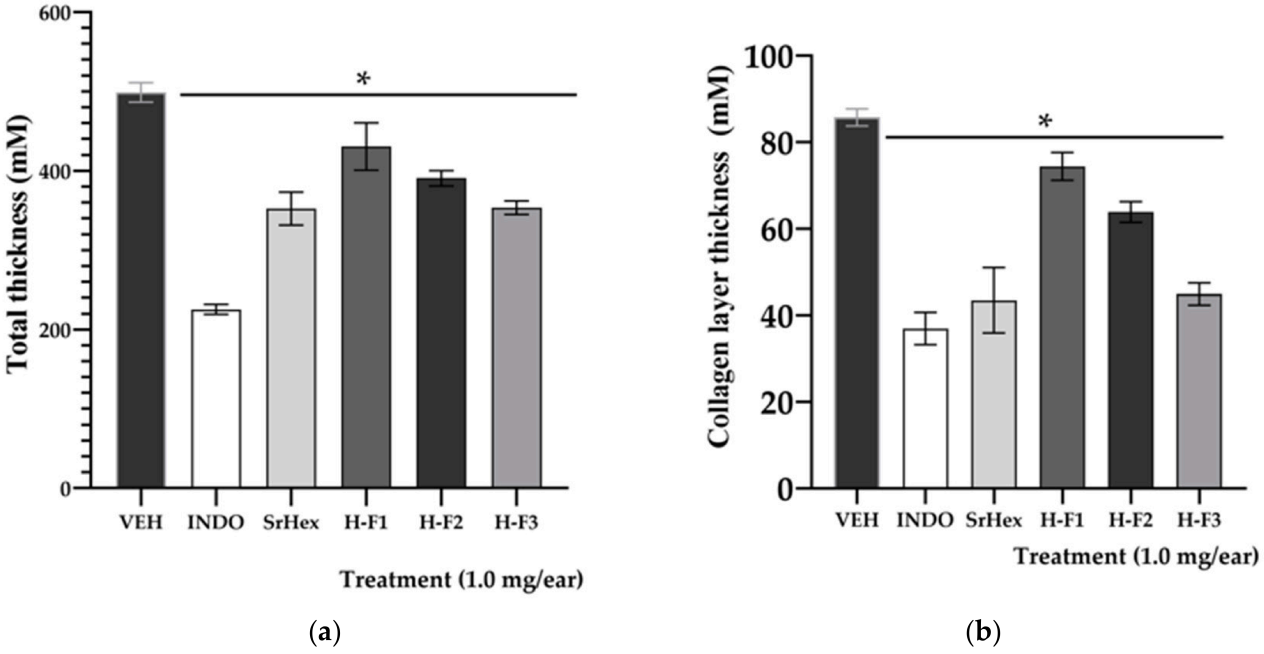
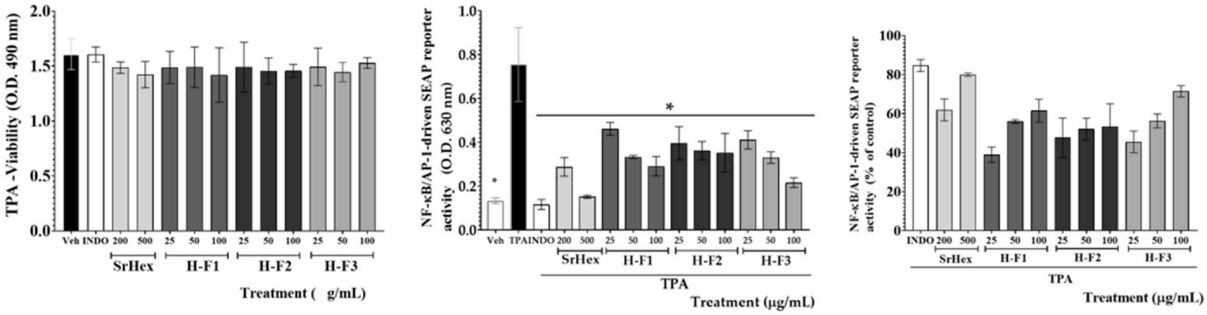


Figure 4. Effect of the local administration of hexane (SrHex) and selected fractions from SrHex: H-F1, H-F2, H-F3 on (**a**) the total thickness of ear observed under microscopy; and (**b**) collagen layer thickness. One way ANOVA and Dunnett's test established a statistically significant difference compared to the VEH group (which only received TPA) when * $p \leq 0.05$. The edema experiment included six animals per group ($n = 6$); histological and morphometric analyses were performed on five stained tissue samples per group ($n = 5$). Data are presented as mean ± SD. * $p \leq 0.05$ versus the VEH group.

3.5. Effects of Sida rhombifolia L. on RAW-Blue™ Macrophage-Derived Cells

3.5.1. *S. rhombifolia* L. on TPA-Stimulated RAW-Blue™ Macrophages

In Figure 5, the effects of the *S. rhombifolia* L. hexane extract (SrHex) and its derived fractions (H-F1, H-F2, and H-F3) on cell viability and TPA-induced NF-κB/AP-1 activation in RAW-Blue™ macrophages are shown. None of the treatments markedly affected RAW-Blue™ cell viability under the experimental conditions evaluated (Figure 5a). Optical density values at 490 nm remained comparable among the vehicle, indomethacin (INDO), SrHex, and H-F1, H-F2, and H-F3 treatment groups, indicating that the inhibitory effects observed in the reporter assay were not associated with a substantial loss of cell viability.



(**a**) (**b**) (**c**)

Figure 5. Effect of the hexane extract of *Sida rhombifolia* L. (SrHex) and its fractions on TPA-stimulated RAW-Blue™ macrophages. (**a**) Cell viability determined by optical density (O.D.) at 490 nm after treatment with SrHex (200 and 500 μg/mL) or its fractions H-F1, H-F2, and H-F3 (25, 50, and 100 μg/mL). (**b**) NF-κB/AP-1-driven SEAP reporter activity, measured by O.D. at 630 nm following TPA stimulation and treatment with SrHex or its fractions. (**c**) Percentage inhibition of NF-κB/AP-1-driven SEAP reporter activity relative to the TPA-stimulated group. Veh, vehicle control; TPA, 12-*O*-tetradecanoylphorbol-13-acetate; INDO, indomethacin; SrHex, hexane extract of *S. rhombifolia*. Data are expressed as the mean ± SD (n = 3). Statistical analysis was performed using one-way ANOVA followed by Dunnett's multiple-comparison test. * $p \leq 0.05$ versus the TPA-stimulated group.

TPA stimulation markedly increased NF-κB/AP-1-driven SEAP reporter activity compared with the vehicle group (Figure 5b). INDO substantially reduced TPA-induced reporter activity. SrHex also decreased SEAP activity at both concentrations tested, with a stronger inhibitory effect observed at 500 μg/mL than at 200 μg/mL.

SrHex-derived fractions also attenuated TPA-induced NF-κB/AP-1 activation. H-F1 showed a concentration-dependent effect, reducing reporter activity from approximately 0.46 O.D. units at 25 μg/mL to approximately 0.29 O.D. units at 100 μg/mL. H-F2 produced a moderate reduction in SEAP activity across the concentration range evaluated, whereas H-F3 showed a progressively greater inhibitory effect as the concentration increased, reaching approximately 0.21 O.D. units at 100 μg/mL. The treatments shown in Figure 5b differed significantly from the TPA-stimulated group ($p \leq 0.05$). When NF-κB/AP-1 inhibition was expressed as a percentage relative to the TPA-stimulated control (Figure 5c), INDO produced approximately 84% inhibition. SrHex resulted in approximately 62% and 80% inhibition at 200 and 500 μg/mL, respectively. H-F1 produced approximately 39%, 56%, and 61% inhibition at 25, 50, and 100 μg/mL, respectively. H-F2 produced approximately 48–53% inhibition across the concentrations evaluated, whereas H-F3 showed approximately 46%, 56%, and 71% inhibition at 25, 50, and 100 μg/mL, respectively.

Overall, SrHex and its derived fractions reduced TPA-induced NF-κB/AP-1 transcriptional activity without substantially compromising RAW-Blue™ cell viability. Among the fractions, H-F3 showed the clearest concentration-dependent inhibition, reaching about 70% at 100 μg/mL.

3.5.2. Effect of the *S. rhombifolia* L. Hexane Extract on LPS-Stimulated RAW-Blue™ Macrophages

The effect of the *S. rhombifolia* L. hexane extract (SrHex) on cell viability and LPS-induced NF-κB/AP-1 activation in RAW-Blue™ macrophages is shown in Figure 6. SrHex treatment at concentrations ranging from 125 to 800 μg/mL did not affect the cell viability (Figure 6a). Optical density values at 490 nm remained close to those observed in the vehicle and LPS groups, indicating that the concentrations evaluated did not induce substantial cytotoxicity under the experimental conditions.

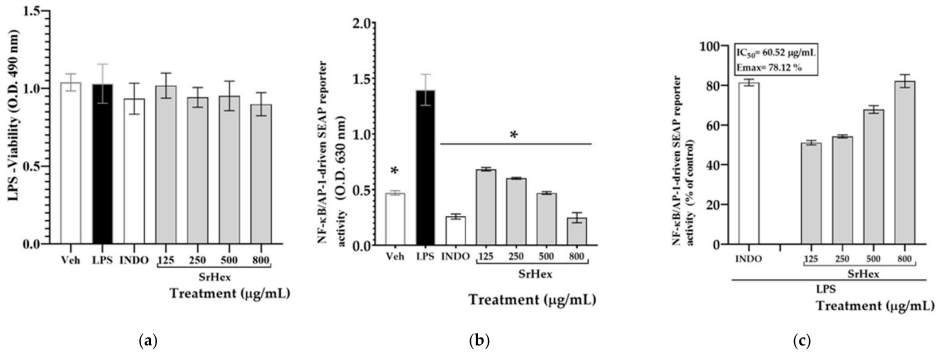


Figure 6. Effect of the hexane extract of *Sida rhombifolia* L. (SrHex) on LPS-stimulated RAW-Blue™ macrophages. (**a**) Cell viability determined by O.D. at 490 nm after treatment with SrHex at 125, 250, 500, and 800 µg/mL. (**b**) NF-κB/AP-1-driven SEAP reporter activity, measured by O.D. at 630 nm following LPS stimulation and treatment with SrHex. (**c**) Percentage inhibition of NF-κB/AP-1-driven SEAP reporter activity relative to the LPS-stimulated group. Veh, vehicle control; LPS, lipopolysaccharide; INDO, indomethacin; SrHex, hexane extract of *S. rhombifolia*. Data are expressed as the mean ± SD (n = 3). Statistical analysis was performed using one-way ANOVA followed by Dunnett's multiple-comparison test. * $p \leq 0.05$ versus the LPS-stimulated group.

LPS stimulation markedly increased NF-κB/AP-1-driven SEAP reporter activity compared with the vehicle group (Figure 6b), reaching an optical density of approximately 1.4 at 630 nm. In contrast, SrHex treatment significantly reduced LPS-induced reporter activity in a concentration-dependent manner. SEAP activity decreased from 0.68 O.D. units to 125 µg/mL to 0.60, 0.46, and 0.24 O.D. units at 250, 500, and 800 µg/mL, respectively.

The highest concentration of SrHex produced reporter activity comparable to that observed with indomethacin (INDO). The indicated treatments were significantly different from the LPS-stimulated group ($p \leq 0.05$). When inhibition was expressed as a percentage relative to the LPS-stimulated group (Figure 6c), SrHex produced approximately 51% inhibition at 125 µg/mL, 54% at 250 µg/mL, 68% at 500 µg/mL, and 82% at 800 µg/mL. INDO produced approximately 81% inhibition under the same experimental conditions. Concentration–response curve fitting yielded an estimated IC_{50} of 60.52 µg/mL and an Emax of 78.12%. Because the estimated IC_{50} was below the lowest experimentally tested concentration (125 µg/mL), this value represents an interpolated model estimate and should be interpreted cautiously.

Overall, SrHex inhibited LPS-induced NF-κB/AP-1 transcriptional activity in a concentration-dependent manner without substantially affecting RAW-Blue™ macrophage viability. At 800 µg/mL, the inhibitory response was comparable to that observed with INDO, supporting a marked suppressive effect of SrHex on LPS-induced NF-κB/AP-1 signaling.

3.5.3. Effect of H-F1, H-F2, H-F3, H-F4, and H-F5 Fractions on LPS-Stimulated RAW-Blue™ Macrophages

H-F1 at 25 µg/mL and 50 µg/mL reduced LPS-induced NF-κB/AP-1-driven SEAP reporter activity without significantly affecting the cell viability signal. At concentrations of 100–800 µg/mL, progressively greater reductions in SEAP reporter activity were observed; however, these concentrations were also associated with a statistically significant reduction in the viability signal. Therefore, the decrease in SEAP activity at 100–800 µg/mL cannot be attributed exclusively to the modulation of NF-κB/AP-1-associated signaling, because reduced cellular viability or metabolic activity may have partially contributed to the observed response (Figure 7a). LPS stimulation markedly increased NF-κB/AP-1-driven SEAP reporter activity, reaching an optical density of approximately 1.4 at 630 nm (Figure 7b). In contrast, treatment with H-F1 progressively decreased SEAP activity in a

concentration-dependent manner. The response decreased to 0.73, 0.63, 0.29, 0.27, 0.16, and 0.03 O.D. units at 25, 50, 100, 200, 400, and 800 µg/mL, respectively. The inhibitory effect of H-F1 was statistically significant compared with the LPS-stimulated group ($p \leq 0.05$).

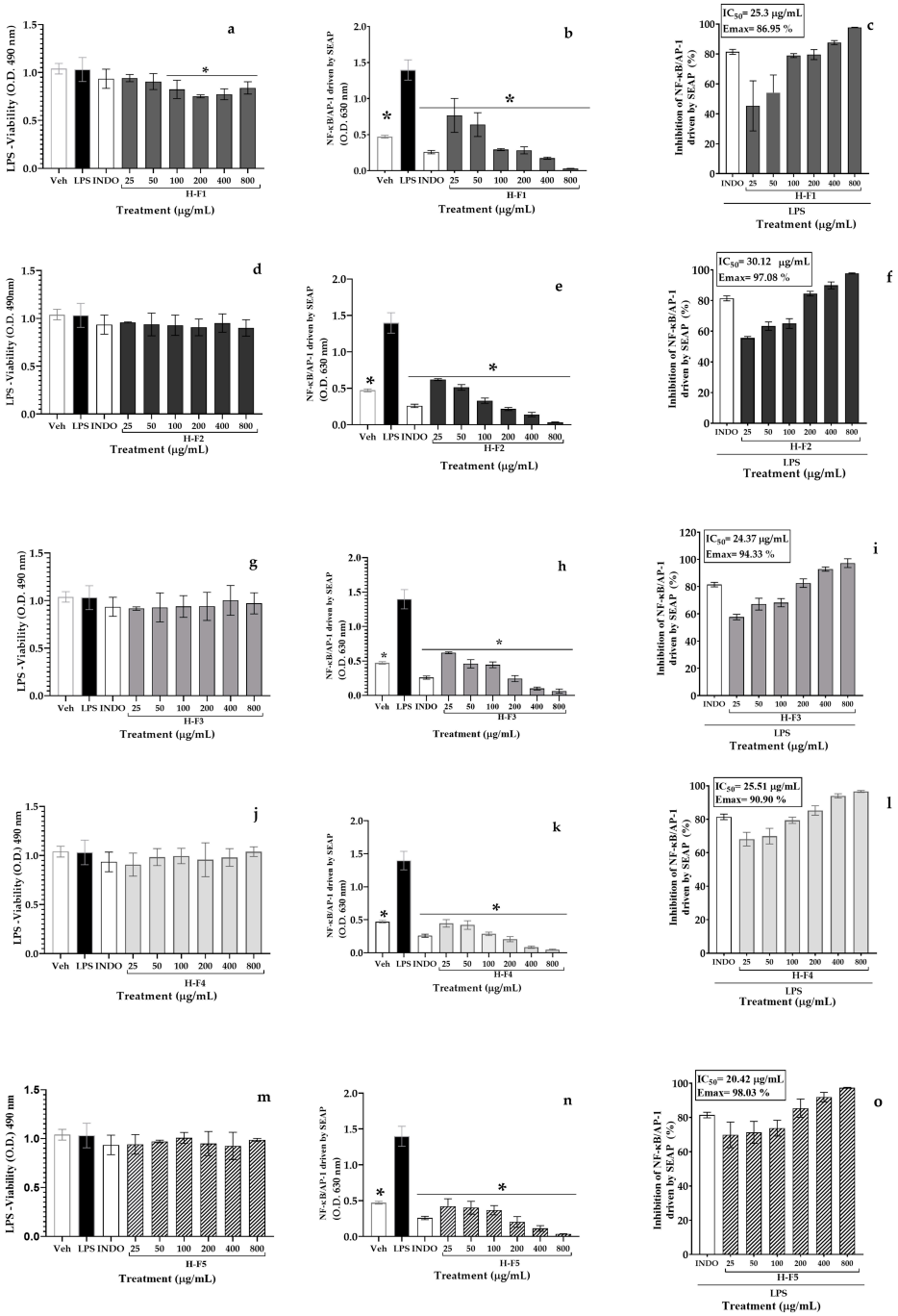


Figure 7. Effects of SrHex-derived fractions H-F1–H-F5 on cell viability and NF-κB/AP-1-driven SEAP reporter activity in LPS-stimulated RAW-Blue™ cells. (**a**–**c**) H-F1; (**d**–**f**) H-F2; (**g**–**i**) H-F3; (**j**–**l**) H-F4; and (**m**–**o**) H-F5. For each fraction, the first panel shows cell viability determined by optical density at 490 nm, the second panel shows NF-κB/AP-1-driven SEAP reporter activity measured at 630 nm following LPS stimulation, and the third panel shows the percentage inhibition of SEAP reporter activity relative to the LPS-stimulated control. Fractions were evaluated at 50, 100, 200, 400, and 800 µg/mL. Veh, vehicle control; LPS, lipopolysaccharide; INDO, indomethacin (200 µg/mL). Data are expressed as the mean ± SD (n = 3). Statistical analysis was performed using one-way ANOVA followed by Dunnett's multiple-comparison test. * $p \leq 0.05$ versus the LPS-stimulated group.

When the inhibitory response was expressed as a percentage relative to the LPS group, H-F1 produced approximately 45.3% and 54% of inhibition at 25 and 50 μg/mL, followed by approximately 67% and 73% inhibition at 100 and 200 μg/mL, respectively (Figure 7c). Higher concentrations produced stronger inhibition, reaching approximately 87.7% at 400 μg/mL and 97.3% at 800 μg/mL. Concentration–response analysis yielded an IC_{50} value of 25.3 μg/mL and a maximum effect (Emax) of 86.95.

Treatment with the H-F2, H-F3, H-F4, and H-F5 fractions did not markedly affect the viability of LPS-stimulated RAW-Blue™ macrophages over the concentration range evaluated (25–800 μg/mL) (Figure 7d,g,j,m). Cell viability remained close to that observed in the vehicle and LPS groups, with O.D. values generally ranging from approximately 0.90 to 1.00 at 490 nm. These results indicate that the inhibitory effects observed on NF-κB/AP-1-driven SEAP reporter activity were not associated with a substantial reduction in cell viability.

Overall, H-F2, H-F3, H-F4, and H-F5 significantly inhibited LPS-induced NF-κB/AP-1-driven SEAP reporter activity without substantially affecting RAW-Blue™ macrophage viability. All fractions showed a concentration-dependent inhibitory response, with maximal inhibition approaching 90–98% at 800 μg/mL. Based on the calculated IC_{50} values, the apparent potency followed the order H-F5 > H-F3 > H-F4 > H-F2, with IC_{50} values of 20.42, 24.37, 25.51, and 30.12 μg/mL, respectively. H-F5 also showed the highest Emax (98.04%), supporting its selection as the most pharmacodynamically active fraction among H-F2 to H-F5.

The H-F2 fraction produced a progressive reduction in LPS-induced NF-κB/AP-1-driven SEAP reporter activity (Figure 7e). LPS stimulation increased reporter activity to approximately 1.4 O.D. units at 630 nm, whereas H-F2 reduced the response to 0.62, 0.51, 0.37, 0.21, 0.14, and 0.0317 O.D. units at 50, 100, 200, 400, and 800 μg/mL, respectively. The indicated treatments were significantly different from the LPS-stimulated group ($p \leq 0.05$). When the inhibitory response was expressed as a percentage relative to the LPS group, H-F2 produced 55.06%, 63.32% and 65.01% of inhibition at 25, 50, and 100 μg/mL, respectively, increasing to 84.92% at 200 μg/mL, 89.88% at 400 μg/mL, and 97.7% at 800 μg/mL (Figure 7f). Concentration–response analysis yielded an IC_{50} value of 30.12 μg/mL and an Emax of 97.08%.

H-F3 also significantly attenuated LPS-induced NF-κB/AP-1 activation in a concentration-dependent manner (Figure 7g). Reporter activity was reduced to 0.59, 0.46, and 0.43 O.D. units at 25, 50, and 100 μg/mL, respectively, and further decreased to approximately 0.25, 0.10, and 0.06 O.D. units at 200, 400, and 800 μg/mL, respectively (Figure 7h).

H-F3 produced 57.64%, 67.11%, and 69.57% inhibition at 25, 50, and 100 μg/mL, respectively, and 82.96% at 200 μg/mL, 92.84% at 400 μg/mL, and 97.20 ± 3.23% at 800 μg/mL. Because the standard deviation was ± 3.23% at this highest concentration, the upper error bar extended to 100.44% in the graph, reflecting statistical dispersion and not inhibition above 100% (Figure 7i). The calculated IC_{50} was 24.37 μg/mL, with an Emax of 94.33%.

Treatment with H-F4 resulted in a marked concentration-dependent inhibition of NF-κB/AP-1-driven SEAP reporter activity following LPS stimulation (Figure 7k). At 25 and 50 μg/mL, reporter activity decreased to 0.45 and 0.42 O.D. units, whereas increasing the concentration to 100, 200, 400, and 800 μg/mL further reduced the response to 0.28, 0.21, 0.08, and 0.05 O.D. units, respectively.

This effect corresponded to 57.0% at 25 μg/mL and 69.90% inhibition at 50 μg/mL, 79.64% at 100 μg/mL, 85.63% at 200 μg/mL, 93.96% at 400 μg/mL, and approximately 96.61% at 800 μg/mL (Figure 7l). In Figure 7i, H-F4 exhibited an IC_{50} of 25.51 μg/mL and an Emax of 90.90%. In this experiment, H-F5 had the strongest inhibitory profile among the fractions evaluated (Figure 7n). NF-κB/AP-1-driven SEAP reporter activity progressively

decreased as the concentration of H-F5 increased, reaching approximately 0.42, 0.40, 0.31, 0.21, 0.11, and 0.04 O.D. units at 50, 100, 200, 400, and 800 μg/mL, respectively.

For H-F5, the percentage of inhibition was 69.83% at 25 μg/mL, 71.29% at 50 μg/mL, 78.14% at 100 μg/mL, 92.12% at 200 μg/mL, 92.96% at 400 μg/mL, and 97.40 ± 0.23% at 800 μg/mL. In contrast to H-F3, the markedly lower standard deviation at 800 μg/mL (±0.23%) resulted in an error bar that remained below the 100% threshold [Figure 7o]. Concentration–response analysis yielded an IC_{50} of 20.42 μg/mL and an Emax of 98.03%, indicating that H-F5 was the most potent fraction based on the IC_{50} values.

4. Discussion

Sida rhombifolia L. has traditionally been used to treat inflammatory conditions, and previous pharmacological studies have provided evidence supporting the anti-inflammatory properties of extracts and metabolites from this species [1–5]. In the present study, the anti-inflammatory activity of *S. rhombifolia* was investigated through complementary in vivo and in vitro approaches. The results demonstrate that the hexane extract (SrHex) and selected fractions attenuated TPA-induced auricular inflammation, improved histopathological alterations associated with the inflammatory response, and reduced NF-κB/AP-1-driven SEAP reporter activity following TPA or LPS stimulation in RAW-Blue™ cells. Together, these observations provide evidence that the non-polar constituents of this species contain pharmacologically active components that can modulate different aspects of the inflammatory response.

The topical TPA-induced ear edema model is widely used to investigate acute inflammation because phorbol esters rapidly induce vascular and tissue alterations, epidermal hyperplasia, inflammatory cell recruitment, oxidative stress, and the activation of intracellular inflammatory signaling [19–22]. TPA-induced responses also involve phospholipase A2 (PLA2), arachidonic acid metabolism, cyclooxygenase-derived mediators, and other signaling processes that contribute to edema and local tissue injury [23–25]. SrHex and its fractions significantly attenuated TPA-induced ear edema, with H-F3 showing the greatest efficacy among fractions, although less potent than indomethacin. A potential limitation of the pretreatment model is that lipophilic extracts may act as a physical barrier to TPA absorption, leading to a false-positive anti-inflammatory effect. To address this, we included two critical controls: mineral oil [10 μL] as a purely lipophilic vehicle followed by TPA, and reverse administration [TPA followed by SrHex 15 min later] (Supplementary Materials). Both approaches demonstrated that TPA-induced inflammation occurs irrespective of vehicle lipophilicity or application sequence, ruling out a non-specific barrier effect and supporting a genuine pharmacological action of SrHex and H-F3.

Importantly, histological evidence supported the macroscopic reduction in edema. TPA-treated vehicle animals showed pronounced epidermal and subcutaneous tissue thickening, inflammatory cell infiltration, disorganization of the reticular dermis, interstitial edema, vascular congestion, and increased thickness of the collagen-containing connective tissue layer. These alterations are consistent with the acute inflammatory changes previously described after topical exposure to TPA [19–22]. Treatment with INDO, SrHex, H-F1, H-F2, and H-F3 attenuated these structural alterations to different degrees, indicating that the anti-edematous response was accompanied by the preservation of tissue architecture.

Morphometric analysis supported the histological findings. SrHex and H-F3 produced the most consistent reductions in epidermal and subcutaneous tissue thickness, suggesting that H-F3 retained constituents contributing to the activity of the parent extract. However, its effects were numerically lower than those of indomethacin, indicating partial attenuation. SrHex and H-F3 also reduced the thickness of the collagen-containing connective tissue layer to values numerically close to indomethacin, whereas H-F1 and H-F2 showed more

modest effects. In this acute TPA model (hours after induction), increased thickness of this layer reflects edema-associated tissue expansion and inflammatory infiltration rather than increased collagen deposition or established fibrosis, which requires long-term extra-cellular matrix remodeling. Therefore, we interpret these changes as reduced edema-associated expansion, not as an antifibrotic effect, and numerical similarity to indomethacin does not establish equivalent efficacy [22]; however, increased layer thickness alone does not demonstrate increased collagen deposition or fibrosis.

Histological findings support the pharmacological relevance of H-F3 by demonstrating activity across complementary experimental endpoints. In addition to reducing TPA-induced ear edema in vivo, H-F3 attenuated epidermal/subcutaneous tissue thickening and thickening of the collagen-containing connective tissue layer. It was also among the most active fractions in reducing SEAP reporter activity in the TPA-stimulated RAW-Blue™ cells. This concordance across macroscopic, histological, and cellular assessments identifies H-F3 as the fraction with the most consistent activity under TPA-stimulated conditions, although it does not establish a shared mechanism of action across these assays.

Previous studies with *S. rhombifolia* are compatible with these findings. Hydroalcoholic preparations from the leaves have been reported to reduce inflammatory responses and promote wound healing [26], while *p*-hydroxyphenethyl *trans*-ferulate isolated from a non-polar extract showed inhibitory activity against TPA-induced edema [26]. Ethanolic preparations of *S. rhombifolia* have also demonstrated anti-inflammatory effects in LPS-induced periapical lesions and carrageenan-induced paw edema models [2,27]. Collectively, these observations indicate that the anti-inflammatory potential of the species is reproducible across different extraction procedures and experimental systems [28].

The RAW-Blue™ reporter assay provided additional information regarding the cellular effects of SrHex and its fractions. In TPA-stimulated cells, SrHex at 500 μg/mL and H-F3 at 100 μg/mL produced the greatest decreases in NF-κB/AP-1-driven SEAP reporter activity. This result is particularly noteworthy because H-F3 was also the most active fraction in the TPA-induced in vivo model. Such concordance suggests that the anti-inflammatory activity of H-F3 may involve the modulation of intracellular signaling pathways activated downstream of TPA exposure. However, the reporter assay does not identify the direct molecular target; therefore, these findings should be interpreted as the modulation of signaling associated with NF-κB/AP-1 activation rather than direct inhibition of either transcription factor [29].

The effects observed following LPS stimulation provide complementary evidence. LPS activates inflammatory signaling through the CD14/TLR4/MD-2 receptor complex, then engages MyD88- and TRIF-dependent pathways, ultimately promoting NF-κB activation and the transcription of inflammatory mediators [29]. SrHex significantly reduced LPS-induced NF-κB/AP-1-driven SEAP reporter activity in a concentration-dependent manner.

Fractionation of SrHex markedly increased apparent potency against LPS-induced reporter activity. Thus, the apparent potency followed the order H-F5 > H-F3 > H-F4 > H-F2 > H-F1 > SrHex, when potency is interpreted inversely according to the IC_{50} value. In addition, several fractions reached maximal inhibition values of approximately 95–98%, indicating that fractionation not only increased apparent potency, but also yielded fractions capable of producing almost complete inhibition of LPS-induced reporter activity.

The RAW-Blue™ SEAP reporter assay provides an indirect measure of signaling associated with NF-κB/AP-1 activation and does not demonstrate direct inhibition of either transcription factor. Therefore, the present findings should be interpreted as evidence of the modulation of NF-κB/AP-1-associated signaling, while confirmation of the specific molecular targets will require additional mechanistic studies [29].

Potency and maximal efficacy differ among the analyzed fractions; thus, H-F5 showed the lowest IC_{50} and therefore the highest potency under LPS-stimulated conditions. Cell viability experiments are important for interpreting these observations. H-F2, H-F3, H-F4, and H-F5 did not substantially alter RAW-Blue™ cell viability across the evaluated concentrations, indicating that their reduction in SEAP reporter activity was not simply attributable to generalized cellular toxicity.

Interpreting the results obtained with H-F1 requires caution. Although it markedly reduced NF-κB/AP-1-mediated SEAP activity, it also significantly decreased the viability signal within the 100 to 800 μg/mL range. Because SEAP production was not normalized to viable cell number or total protein content, we cannot rule out that reduced viability contributed to the decrease in SEAP signal at these concentrations. However, at 50 μg/mL, H-F1 inhibited SEAP activity by approximately 54% without significantly affecting viability, providing evidence of reporter-gene modulation independent of cytotoxicity. To definitively characterize H-F1, use lower concentration ranges and normalize SEAP levels to viability or protein content.

One of the most relevant findings of this study is the different biological behavior exhibited by H-F3 and H-F5. H-F3 showed the strongest and most consistent activity in the TPA-induced in vivo model, histological analysis, and the TPA-stimulated cellular assay [30–32], whereas H-F5 displayed the highest apparent potency in LPS-stimulated RAW-Blue™ cells but showed no comparable activity in the in vivo TPA model [30,33]. This divergence should not necessarily be considered contradictory. Rather, it indicates that each fraction's pharmacological response depends on the inflammatory stimulus, chemical content, and biological context.

The topical in vivo model includes several processes absent from an isolated cellular reporter assay, including penetration through the skin barrier, local distribution, tissue retention, metabolism, vascular effects, recruitment of inflammatory cells, and interactions among multiple cell populations. Conversely, the RAW-Blue™ assay predominantly reflects changes in reporter signaling downstream of a defined inflammatory stimulus [29]. Therefore, the pronounced in vitro activity of H-F5 may reflect the potent modulation of LPS-activated signaling without necessarily predicting favorable topical bioavailability or activity against TPA-induced tissue inflammation [30].

Similarly, the consistent activity of H-F3 against TPA in vivo and in vitro suggests that its constituents may possess physicochemical and pharmacological properties that favor activity in the skin environment in addition to affecting intracellular inflammatory signaling. This hypothesis should nevertheless be evaluated directly through future studies addressing tissue penetration, local pharmacokinetics, and molecular targets.

GC-MS analysis provided a preliminary chemical profile of H-F3 and H-F5. H-F3 contained three major constituents identified as dihydroactinidiolide [34–39], 2-methylene-5α-cholestan-3β-ol, and hexanedioic acid, mono(2-ethylhexyl) ester. H-F5 was initially characterized with this methodology, and preliminary analysis indicates that it contains cyclopropane tetradecanoic acid, 2-octyl-methyl ester, and 3′,8,8′-trimethoxy-3-piperidyl-2,2′-binaphthalene-1,1′,4,4′-tetrone. The identified compounds were neither isolated nor confirmed using analytical standards, and their individual pharmacological activities were not evaluated. Consequently, another limitation of this study is that the biological effects observed in H-F3 and H-F5 cannot be conclusively attributed to dihydroactinidiolide or to any other individual constituent detected in these fractions. Although dihydroactinidiolide was identified in H-F3 and appeared to be a predominant constituent, current data do not support designating it as the active principle responsible for the observed pharmacological effects. Therefore, the GC-MS results should be considered preliminary compositional evidence supporting the chemical characterization of H-F3 and H-F5. Still, they do not

establish a causal relationship between any specific compound and the observed biological activity. Further studies involving isolation, structural confirmation, and the evaluation of individual constituents are required to determine their respective contributions to the pharmacological effects of these fractions. Bioassay-guided isolation, structural confirmation, and individual pharmacological evaluation of the isolated constituents will be required to determine whether any specific compound contributes to the biological activity of these fractions.

A limitation of the NF-κB/AP-1-regulated SEAP reporter gene assays is that they provide an indirect readout of inflammatory signaling and do not identify the specific molecular targets of SrHex or its fractions. Consequently, current data support the modulation of pathways associated with NF-κB/AP-1 activation but do not demonstrate direct inhibition of NF-κB, AP-1, TLR4, PKC, or other individual components. Furthermore, soluble phytochemicals cannot be formally ruled out as directly interfering with the assay. Although the samples were lyophilized to remove organic solvents, dispersed in 0.002% Tween 20, sonicated, filtered through a 40 µm sieve, and only cell-free supernatants were analyzed using QUANTI-Blue™, residual soluble constituents could theoretically interfere with SEAP detection. Nevertheless, vehicle controls performed in parallel, the dose-dependent response, and consistent activity across independent preparations suggest that this is not a non-specific chemical artifact. Such constituents could potentially affect SEAP enzymatic activity or interact directly with the QUANTI-Blue™ colorimetric reaction, thereby influencing the absorbance measured at 630 nm independently of changes in NF-κB/AP-1-associated signaling. Because a cell-free interference control containing SEAP and the corresponding extract or fraction was not performed, this possibility cannot be completely ruled out and should be considered when interpreting the reporter assay results. Future studies should include appropriate cell-free controls to determine whether the tested samples directly affect SEAP activity or QUANTI-Blue™ color development.

Also, the study did not evaluate skin penetration, local tissue distribution, stability, metabolism, or the fractions' pharmacokinetic behavior. These factors may contribute to the differences observed between the topical TPA model and the RAW-Blue™ cellular assays.

Although H-F2 and H-F5 did not substantially affect cell viability under the conditions tested, the present experiments do not constitute a complete toxicological assessment. In addition, the reduction in viability observed with H-F1 at higher concentrations limits the interpretation of its SEAP response at these concentrations.

Finally, direct mechanistic studies, including evaluation of p65 nuclear translocation, IκBα phosphorylation/degradation, and inflammatory mediators such as TNF-α, IL-6, IL-1β, NO, PGE_2, COX-2, and iNOS, are needed to identify the specific pathways affected by the active fractions.

Taken together, the present results show that SrHex and its derived fractions exhibit different biological profiles depending on the experimental model. H-F3 produced the greatest numerical inhibition of TPA-induced auricular edema and showed consistent effects in the histological and TPA-stimulated cellular evaluations. H-F5 also significantly reduced TPA-induced edema, although to a lesser extent, and showed the lowest IC_{50} in the LPS-stimulated RAW-Blue™ reporter assay. These findings support further investigation of both fractions, but additional mechanistic, phytochemical, pharmacokinetic, and toxicological studies are needed before assigning their biological effects to specific compounds or molecular targets.

5. Conclusions

This study validates the anti-inflammatory potential of *S. rhombifolia* L. and demonstrates that its hexane extract comprises fractions with distinct profiles. H-F3 showed the

most consistent activity across models, significantly reducing TPA-induced ear edema in vivo, attenuating inflammatory histological markers, and inhibiting TPA-driven NF-κB/AP-1 SEAP reporter activity in RAW-Blue™ cells.

In contrast, H-F5 displayed the highest potency against LPS-induced NF-κB/AP-1 activation. These divergent profiles suggest that the anti-inflammatory effects of *S. rhombifolia* are not mediated by a single compound but rather by chemically distinct constituents whose activity depends on the inflammatory trigger. The compounds tentatively identified in H-F3 and H-F5 (Figure 8) may contribute to these effects; however, confirming their specific roles and molecular mechanisms requires isolating individual metabolites and validating direct targets.

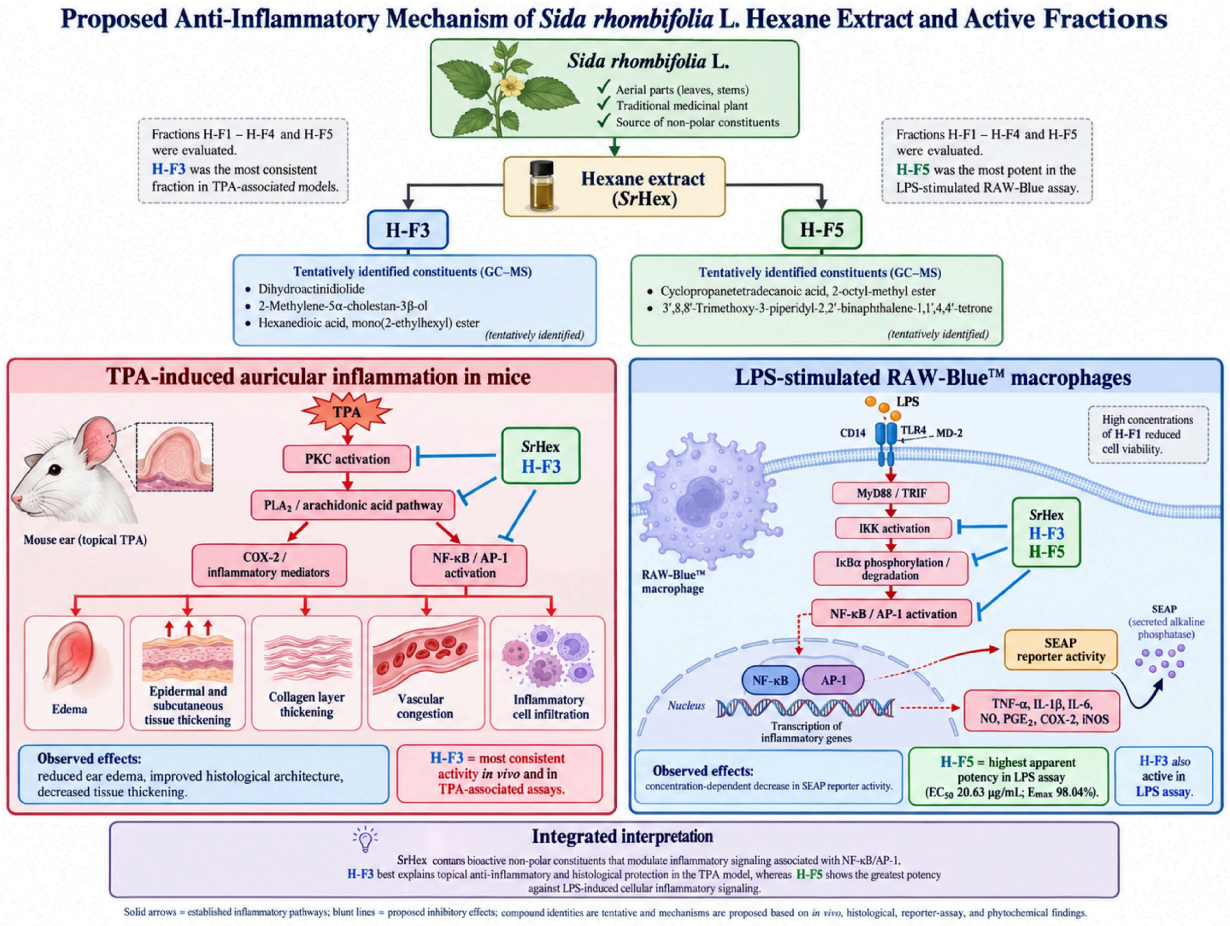


Figure 8. Schematic representation of the effect of *S. rhombifolia*. This figure proposes a possible anti-inflammatory mode of action for the representative treatments of the species analyzed. TPA = 12-*O*-tetradecanoylphorbol-13-acetate; PKC = protein kinase C signaling; PLA_2 = phospholipase A; COX-2 = cyclooxygenase-2; NF-κB = nuclear factor kappa B; AP-1 = activator protein 1; LPS = lipopolysaccharide; CD14 = cell surface antigen CD14; TLR4 = toll-like receptor 4; MD-2 = molecule requisite for LPS signaling of TLR4; MyD88 = canonical adaptor for inflammatory signaling pathways downstream of members of the toll-like receptor (TLR) and interleukin-1 (IL-1) receptor families; TRIF = a key adaptor for TLR3 and TLR4 signaling and is primarily responsible for viral (and bacterial) stimulation via the induction of type I interferons (IFNs) including IFNα, IFNβ, and other IFNs; IKK = I kappa B kinase is a regulatory subunit that plays a crucial role in the activation of the IKK complex, which is responsible for phosphorylating inhibitor molecules to release active NF-κB; SEAP = secreted embryonic alkaline phosphatase; TNF-α = interferon alpha; IL-1β = interleukine-1 beta; IL-6 = interleukine-6, NO = nitric oxide, PGE_2 = prostaglandin E-2; iNOS = inducible nitric oxide synthase. Created in BioRender. Zapata, M. (2026). https://BioRender.com/nxctzaa.

Supplementary Materials: The following supporting information can be downloaded at: https://www.mdpi.com/article/10.3390/cimb48111094/s1.

Author Contributions: Conceptualization, M.H.-R., N.M.-B. and E.J.-F.; methodology, M.H.-R. and N.M.-B.; formal analysis, M.H.-R. and E.J.-F.; investigation, V.B.-S. and Y.M.Z.-L.; chemical analysis, M.G.-C.; resources, M.H.-R., N.M.-B. and E.J.-F.; plant collection and taxonomic identification, G.F.-F.; histologic analysis N.M.-B.; microscopy for histology imaging D.T.-M.; writing—original draft preparation, M.H.-R. and N.M.-B.; writing—review and editing, E.J.-F. and G-C M.; project administration, N.M.-B.; funding acquisition, M.H.-R., N.M.-B. and E.J.-F. All authors have read and agreed to the published version of the manuscript.

Funding: This research was funded by the SECIHTI (Secretaría de Ciencia, Humanidades, Tecnología e Innovación) through resources allocated to project CF-2023-G-1508, and the APC was funded by these resources.

Institutional Review Board Statement: The study was conducted in accordance with the Declaration of Helsinki, and approved by the Institutional Animal Care and Use Committee (CICUAL) of the Southern Biomedical Research Center (CICUAL-CIBIS)) (protocol code R-CICUAL-2024-06, approval date: 28 June 2024).

Informed Consent Statement: Not applicable.

Data Availability Statement: No new data were created or analyzed in this study. Data sharing is not applicable to this article.

Acknowledgments: We thank Xochitl de Jesús M (DVM) and Duanivan Carnalla for their technical contribution to the handling of laboratory animals.

Conflicts of Interest: The authors declare no conflicts of interest, and the funders had no role in the design of the study; in the collection, analyses, or interpretation of data; in the writing of the manuscript; or in the decision to publish the results.

References

1. Jiménez-Ferrer, E.; Herrera-Ruiz, M.; Campos-Vidal, Y.; Flores-Franco, G.; Monterrosas-Brisson, N. *Sida* L.: Ethnobotany, Pharmacology, and Phytochemistry: A Review. *Plants* **2025**, *14*, 3115. [CrossRef] [PubMed]
2. Tanumihadja, M.; Natsir, N.; Mattulata, I.K.; Lukman, M. Potent anti-inflammatory effect of root of sidaguri (*Sida rhombifolia* L.) on rat periapical lesion model. *Int. J. Toxicol. Pharm. Res.* **2016**, *8*, 412–415.
3. Tanumihardja, M.; Mattulada, I.K.; Natsir, N.; Subehan, S.; Mandey, F.; Muslimin, L. Structural assessment of chemical constituent of sidaguri (*Sida rhombifolia* Linn) and its ability to inhibit cyclooxygenase. *Pesqui. Bras. Odontopediatria Clín. Integr.* **2019**, *19*, e4773. [CrossRef]
4. Azad, A.K.; Islam, O.; Khairuzzaman, M.; Ferdous, J.; Shaheen, S.M. Hypoglycemic, analgesic and anti-inflammatory activities of methanol extract of *Sida rhombifolia* L. leaves on experimental mice. *Int. J. Pharma Sci. Sci. Res.* **2017**, *3*, 82–87. [CrossRef]
5. Mah, S.H.; Teh, S.S.; Ee, G.C.L. Anti-inflammatory, anti-cholinergic and cytotoxic effects of *Sida rhombifolia*. *Pharm. Biol.* **2017**, *55*, 920–928. [CrossRef] [PubMed]
6. Chen, L.; Deng, H.; Cui, H.; Fang, J.; Zuo, Z.; Deng, J.; Li, Y.; Wang, X.; Zhao, L. Inflammatory responses and inflammation-associated diseases in organs. *Oncotarget* **2018**, *9*, 7204–7218. [CrossRef] [PubMed]
7. Chelangarimiyandoab, F.; Lavoie, J.-P.C.; Flamand, N.; Cordat, E.; Breton, S. Molecular mechanisms of acute inflammation: Systemic responses and kidney-specific pathophysiology. *Function* **2026**, *7*, e0872025. [CrossRef] [PubMed]
8. Medzhitov, R. Origin and physiological roles of inflammation. *Nature* **2008**, *454*, 428–435. [CrossRef] [PubMed]
9. Furman, D.; Campisi, J.; Verdin, E.; Carrera-Bastos, P.; Targ, S.; Franceschi, C.; Ferrucci, L.; Gilroy, D.W.; Fasano, A.; Miller, G.W.; et al. Chronic inflammation in the etiology of disease across the life span. *Nat. Med.* **2019**, *25*, 1822–1832. [CrossRef] [PubMed]
10. Soysal, P.; Arik, F.; Smith, L.; Jackson, S.E.; Isik, A.T. Inflammation, Frailty and Cardiovascular Disease. In *Frailty and Cardiovascular Diseases. Advances in Experimental Medicine and Biology*; Veronese, N., Ed.; Springer International Publishing AG: Cham, Switzerland, 2020; Volume 1216, pp. 55–64. [CrossRef] [PubMed]
11. Zhang, J.; Fu, L.; Shi, J.; Chen, X.; Li, Y.; Ma, B.; Zhang, Y. The risk of metabolic syndrome in patients with rheumatoid arthritis: A meta-analysis of observational studies. *PLoS ONE* **2013**, *25*, e78151. [CrossRef] [PubMed]
12. Zhang, Z.; Zhao, L.; Zhou, X.; Meng, X.; Zhou, X. Role of inflammation, immunity, and oxidative stress in hypertension: New insights and potential therapeutic targets. *Front. Immunol.* **2023**, *13*, 1098725. [CrossRef] [PubMed]

13. Deleidi, M.; Jaggle, M.; Rubino, G. Immune aging, dysmetabolism, and inflammation in neurological diseases. *Front. Neurosci.* **2015**, *9*, 172. [CrossRef] [PubMed]
14. Singh, D. Astrocytic and microglial cells as the modulators of neuroinflammation in Alzheimer's disease. *J. Neuroinflammation* **2022**, *19*, 206. [CrossRef] [PubMed]
15. Cuevas-Mancilla, V.M.; López, P.A.; López-Sánchez, H.; Ríos-Cortés, A.M.; Gil-Muñoz, A.; Montiel-Ruiz, R.M.; González-Cortazar, M. Chemical Profile of *Bacopa procumbens* and Its Antinociceptive Effect. *Future Pharmacol.* **2026**, *6*, 16. [CrossRef]
16. *NOM-062-ZOO-1999*; DE LOS ANIMALES, C. Y. U. NORMA Oficial Mexicana, Especificaciones Técnicas Para la Producción, Cuidado y uso de los Animales de Laboratorio. Diario Oficial de la Federación: Ciudad de Mexico, Mexico, 1999.
17. Payá, M.; Ferrándiz, M.L.; Sanz, M.J.; Bustos, G.; Blasco, R.; Rios, J.L. Study of the anti-oedema activity of some seaweed and sponge extracts from the mediterranean coast in mice. *Phytother. Res.* **1993**, *7*, 159–162. [CrossRef]
18. Azkona, G. Implementing the 3Rs in Laboratory Animal Research-From Theory to Practice. *Animals* **2023**, *13*, 3063. [CrossRef] [PubMed]
19. De Vry, C.G.; Valdez, M.; Lazarov, M.; Muhr, E.; Buelow, R.; Fong, T.; Iyer, S. Topical application of a novel immunomodulatory peptide, RDP58, reduces skin inflammation in the phorbol ester-induced dermatitis model. *J. Invest. Dermatol.* **2005**, *125*, 473–481. [CrossRef] [PubMed]
20. Stanley, P.L.; Steiner, S.; Havens, M.; Tramposch, K.M. Mouse skin inflammation induced by multiple topical applications of 12-O-tetradecanoylphorbol-13-acetate. *Ski. Pharmacol.* **1991**, *4*, 262–271. [CrossRef] [PubMed]
21. Rakariyatham, K.; Du, Z.; Yuan, B.; Gao, Z.; Song, M.; Pan, C.; Han, Y.; Wu, X.; Tang, Z.; Zhang, G.; et al. Inhibitory effects of 7,7′-bromo-curcumin on 12-O-tetradecanoylphorbol-13-acetate-induced skin inflammation. *Eur. J. Pharmacol.* **2019**, *858*, 172479. [CrossRef] [PubMed]
22. Wu, X.; Song, M.; Rakariyatham, K.; Zheng, J.; Wang, M.; Xu, F.; Gao, Z.; Xiao, H. Inhibitory Effects of 4′-Demethylnobiletin, a Metabolite of Nobiletin, on 12-O-Tetradecanoylphorbol-13-acetate (TPA)-Induced Inflammation in Mouse Ears. *J. Agric. Food Chem.* **2015**, *63*, 10921–10927. [CrossRef] [PubMed]
23. Lu, P.; Takai, K.; Weaver, V.M.; Werb, Z. Extracellular matrix degradation and remodeling in development and disease. *Cold Spring Harb. Perspect. Biol.* **2011**, *3*, a005058. [CrossRef] [PubMed]
24. Murakami, M.; Sato, H.; Taketomi, Y. Updating Phospholipase A_2 Biology. *Biomolecules* **2020**, *10*, 1457. [CrossRef] [PubMed]
25. Otuki, M.F.; Schwob, O.; Silveira-Prudente, A.; Zaltsman, I.; Meretski, S.; Segal, J.; Yedgar, S.; Rosenblat, G. Attenuation of experimental TPA-induced dermatitis by acetylenic acetogenins is associated with inhibition of PLA_2 activity. *Eur. J. Pharmacol.* **2011**, *672*, 175–179. [CrossRef] [PubMed]
26. Loutfi, Y.; Xavier, V.D.; Stephanie, R.M.; Francelline, R.J. Évaluation de l'effet cicatrisant de *Sida rhombifolia* (malvaceae) sur les plaies cutanées chez la souris. *RSTE* **2020**, *2*, 122–129.
27. Kumar, A.; Mishra, P.G.; Tomar, S.D.; Pathak, M.; Pandey, K.R.; Singh, L. Phyto-therapeutic potential of aerial part of *Sida rhombifolia* for antiinflammatory, antinociceptive, and antioxidant activity. *Int. J. Pharm. Qual. Assur.* **2023**, *14*, 91–95. [CrossRef]
28. Arciniegas, A.; Pérez-Castorena, A.L.; Nieto-Camacho, A.; Kita, Y.; Vivar, A.R.D. Anti-hyperglycemic, antioxidant, and anti-inflammatory activities of extracts and metabolites from *Sida acuta* and *Sida rhombifolia*. *Quim. Nova* **2017**, *40*, 176–181. [CrossRef]
29. Yedgar, S.; Cohen, Y.; Shoseyov, D. Control of phospholipase A2 activities for the treatment of inflammatory conditions. *Biochim. Biophys. Acta.* **2006**, *1761*, 1373–1382. [CrossRef] [PubMed]
30. Arroyo-Xochihua, O.; Zepeda, R.C.; Sánchez-Medina, A. RAW 264.7 macrophage cell line as a metabolomic model for analyzing and understanding inflammation processes. *Naunyn-Schmiedeberg's Arch. Pharmacol.* **2026**, *399*, 9527–9549. [CrossRef] [PubMed]
31. Veh, J.; Mangold, C.; Felsen, A.; Ludwig, C.; Gerstner, L.; Reinhardt, P.; Schrezenmeier, H.; Fabricius, D.; Jahrsdörfer, B. Phorbol-12-myristate-13-acetate is a potent enhancer of B cells with a granzyme B+ regulatory phenotype. *Front. Immunol.* **2023**, *14*, 1194880. [CrossRef] [PubMed]
32. Lu, Y.C.; Yeh, W.C.; Ohashi, S.P. LPS/TLR4 signal transduction pathway. *Cytokine* **2008**, *42*, 145–151. [CrossRef] [PubMed]
33. Chuang, L.T.; Shih, Y.H.; Huang, W.C.; Lin, L.C.; Hsu, C.; Chyuan, J.H.; Tsai, T.H.; Tsai, P.J. In vitro and in vivo screening of wild bitter melon leaf for anti-inflammatory activity against *Cutibacterium acnes*. *Molecules* **2020**, *25*, 4277. [CrossRef] [PubMed]
34. Rodríguez-Mesa, X.M.; Contreras Bolaños, L.A.; Modesti Costa, G.; Mejia, A.L.; Santander González, S.P. A *Bidens pilosa* L. Non-Polar Extract Modulates the Polarization of Human Macrophages and Dendritic Cells into an Anti-Inflammatory Phenotype. *Molecules* **2023**, *28*, 7094. [CrossRef] [PubMed]
35. Das, M.; Devi, K.P. Dihydroactinidiolide regulates Nrf2/HO-1 expression and inhibits caspase-3/Bax pathway to protect SH-SY5Y human neuroblastoma cells from oxidative stress induced neuronal apoptosis. *Neurotoxicology* **2021**, *84*, 53–63. [CrossRef] [PubMed]
36. Das, M.; Balan, D.J.; Kasi, P.D. Mitigation of oxidative stress with dihydroactinidiolide, a natural product against scopolamine-induced amnesia in Swiss albino mice. *Neurotoxicology* **2021**, *86*, 149–161. [CrossRef] [PubMed]
37. Osman, N.A.; Arooj, M.; Kang, H.K.; Hyun, J.W.; Koh, Y.S. Chemical composition, antioxidant, and anti-inflammatory properties of the extracts of *Hormophysa triquetra* and *Padina gymnospora*. *Nat. Prod. Commun.* **2024**, *19*, 1–11. [CrossRef]

38. Hotmian, E.; Ma'ruf, N.; Tania, A.; Suoth, E.; Umar, F.; Tallei, T. Evaluating the immunomodulatory properties of *Cyperus rotundus* tuber's bioactive compounds using a molecular docking approach. *AIP Conf. Proc.* **2022**, *2638*, 070004. [CrossRef]
39. Eyasu, M.; Benedí, J.; Romero, J.A.; Martín-Aragón, S. Antioxidant and Antibacterial Activities of Selected Medicinal Plants from Addis Ababa against MDR-Uropathogenic Bacteria. *Int. J. Mol. Sci.* **2024**, *25*, 10281. [CrossRef] [PubMed]

Disclaimer/Publisher's Note: The statements, opinions and data contained in all publications are solely those of the individual author(s) and contributor(s) and not of MDPI and/or the editor(s). MDPI and/or the editor(s) disclaim responsibility for any injury to people or property resulting from any ideas, methods, instructions or products referred to in the content.